

This is the author's peer reviewed, accepted manuscript. However, the online version of record will be different from this version once it has been copyedited and typeset.

PLEASE CITE THIS ARTICLE AS DOI: 10.1063/5.0332733

1
2
3
4
5
6
7
8
9
10
11
12
13
14
15
16

High Schottky barrier formation in tilted-dipole PdCoO₂/β-Ga₂O₃ (001) interfaces

Takayuki Harada^{1,a}, Takuro Nagai², Kohei Sasaki³

¹ International Center for Materials Nanoarchitectonics (MANA), National Institute for Materials Science, Tsukuba, Ibaraki 305-0044, Japan.

² Electron Microscopy Unit, National Institute for Materials Science; Tsukuba, Ibaraki 305-0044, Japan.

³ Novel Crystal Technology Inc., 2-3-1 Hirose-dai, Sayama, Saitama 350-1328, Japan

^aAuthor to whom correspondence should be addressed: HARADA.Takayuki@nims.go.jp

This is the author's peer reviewed, accepted manuscript. However, the online version of record will be different from this version once it has been copyedited and typeset.

PLEASE CITE THIS ARTICLE AS DOI: 10.1063/5.0332733

Abstract

We report the growth and Schottky junction characteristics of metallic delafossite $\text{PdCoO}_2/\beta\text{-Ga}_2\text{O}_3$ (001) heterostructures. The PdCoO_2 thin films predominantly grow with the epitaxial relationship PdCoO_2 (006) // $\beta\text{-Ga}_2\text{O}_3$ (202), forming a high-quality oxide-oxide interface. Despite a 24° tilt between the PdCoO_2 surface polarization axis and the $\beta\text{-Ga}_2\text{O}_3$ (001) surface normal, a large Schottky barrier height of $\phi_b^{\text{JV}} > 1.7$ eV was achieved. This value is comparable with that reported for $\text{PdCoO}_2/\beta\text{-Ga}_2\text{O}_3$ ($\bar{2}01$) where the PdCoO_2 surface polarization axis is perpendicular to the interface. The $\text{PdCoO}_2/\beta\text{-Ga}_2\text{O}_3$ (001) Schottky junctions showed a large on-off ratio of $\sim 10^8$ at 573 K. These results demonstrate the feasibility of delafossite-type electrodes for $\beta\text{-Ga}_2\text{O}_3$ (001) heterostructures with high-quality homoepitaxial $\beta\text{-Ga}_2\text{O}_3$ layers.

This is the author's peer reviewed, accepted manuscript. However, the online version of record will be different from this version once it has been copyedited and typeset.

PLEASE CITE THIS ARTICLE AS DOI: 10.1063/5.0332733

β -Ga₂O₃ is an ultra-wide-bandgap (UWBG) semiconductor with an energy gap of approximately 4.6–5.0 eV, belonging to the monoclinic system (*C2/m*).¹ It is estimated to have a high critical electric field ($\sim 8 \text{ MV}\cdot\text{cm}^{-1}$), high chemical stability, and melt-growth capability that enables large-diameter single-crystal wafers in a potentially low-cost scheme.¹ These properties make β -Ga₂O₃ a promising candidate for next-generation power devices such as Schottky barrier diodes (SBDs) and field-effect transistors (FETs).

High-temperature electronics is one of the promising applications of β -Ga₂O₃ where the large band gap of β -Ga₂O₃ may help suppress thermal excitation of carriers.² In high-temperature operation of β -Ga₂O₃ devices, large Schottky barrier height (SBH) has merit to suppress leakage and better reverse blocking properties. To this end, oxide electrodes with intrinsically high work functions and/or strong interfacial dipoles have been explored.^{3,4} Among them, delafossite-type metallic oxides *ABO*₂ such as PdCoO₂, PdCrO₂, PdRhO₂, and PtCoO₂ exhibit metallic conductivity and layered crystal structures shown in Fig. 1(a), consisting of alternating *A*⁺ and [*BO*₂][−] layers stacked along the *c*-axis.^{5,6,7} These materials enable surface dipole-driven modulation of electronic states.⁸ At *ABO*₂–semiconductor interfaces, the surface dipole significantly influences the band alignment between the *ABO*₂ and the semiconductor.⁴ Previous studies have demonstrated that PdCoO₂, PdCrO₂, and PdRhO₂ electrodes on β -Ga₂O₃ ($\bar{2}01$) have dipole-driven enhancement of SBH.^{4,9–11} In particular, large SBH of $\sim 1.8 \text{ eV}$ has been obtained in PdCoO₂/ β -Ga₂O₃ ($\bar{2}01$) interface.⁴ The interface dipole arises from the alternating stacking of ionic Pd⁺ and [CoO₂][−] layers.^{7,12} Consistent with the interface dipole picture, scanning tunneling microscopy on bulk crystals has revealed that the work function of PdCoO₂ is strongly dependent on the local termination layer of the cleaved surface, indicating the values for Pd-terminated surface $\phi_{\text{m}}^{\text{Pd}} = 4.7 \text{ eV}$ and for CoO₂-terminated surfaces $\phi_{\text{m}}^{\text{CoO}_2} = 7.8 \text{ eV}$.¹³ The high $\phi_{\text{m}}^{\text{CoO}_2}$ could be consistent with the experimentally observed high SBH in PdCoO₂/ β -Ga₂O₃ ($\bar{2}01$) interface where PdCoO₂ is dominantly terminated with CoO₂ layer at the interface.^{4,9,10,14}

This is the author's peer reviewed, accepted manuscript. However, the online version of record will be different from this version once it has been copyedited and typeset.

PLEASE CITE THIS ARTICLE AS DOI: 10.1063/5.0332733

52 PdCoO₂ thin films have been grown by pulsed laser deposition,^{15,16} molecular beam epitaxy,¹⁷
53 solution-based process,¹⁸ and reactive sputtering¹⁹ mostly on c-plane Al₂O₃ substrates. So far,
54 growth of PdCoO₂ on β -Ga₂O₃ has been limited to ($\bar{2}$ 01) orientations.^{4,9,10} The ($\bar{2}$ 01) orientation
55 of β -Ga₂O₃, however, tends to introduce twins in epitaxial layers, which can degrade device
56 breakdown performance.²⁰ The β -Ga₂O₃ (001), on the other hand, allows high-quality epitaxial
57 growth of homoepitaxial β -Ga₂O₃ and is more suitable for high-power application.²⁰ In this study,
58 we investigate the growth of PdCoO₂ on β -Ga₂O₃ (001) and evaluate its interface structure and
59 Schottky properties.

60 On *n*-type β -Ga₂O₃ (001) substrates doped with Sn ($N_D \sim 1 \times 10^{18} \text{ cm}^{-3}$), an 11- μm thick Cl-
61 doped β -Ga₂O₃ epitaxial layer ($N_D \sim 1 \times 10^{16} \text{ cm}^{-3}$) was grown by halide vapor phase epitaxy
62 (HVPE).²¹ PdCoO₂ thin films ($\sim 30 \text{ nm}$) were subsequently deposited by pulsed laser deposition
63 (PLD)¹⁵ at a substrate temperature of 660 °C under an oxygen pressure of 150 mTorr. The fourth
64 harmonic of an Nd:YAG laser was used to ablate a spark plasma-sintered PdCoO₂ target with the
65 repetition rate of 5 Hz. The thickness of the PdCoO₂ films was controlled by the number of
66 Nd:YAG laser pulses, based on the deposition rate determined on c-plane sapphire substrates.

67 The crystal structure of the PdCoO₂ thin films was characterized by x-ray diffraction (XRD).
68 For selected samples, Au/Ni layers were deposited by electron-beam evaporation on the
69 PdCoO₂/ β -Ga₂O₃ heterostructures to enhance lateral current spreading in the Schottky contact.
70 Circular mesa structures with diameters of $D = 100\text{--}300 \text{ }\mu\text{m}$ were defined by photolithography
71 and reactive ion etching (RIE) using a mixture of Ar and BCl₃ gases. After RIE, the samples were
72 immersed in 35 wt% HCl for 5 min to remove possible damaged layers on the sidewalls of the
73 mesas,²² followed by rinsing in deionized water and isopropanol.

74 Ohmic contacts were formed by depositing Au (200 nm)/Ti (50 nm) on the backside of the
75 Sn-doped β -Ga₂O₃ substrates, resulting in a vertical Schottky diode configuration. Current
76 density–voltage (J – V) characteristics were measured using an Agilent 4155B semiconductor

parameter analyzer with tungsten probes connected via triaxial cables. Capacitance–voltage ($C-V$) measurements were carried out using an Agilent E4980A LCR meter by applying a 1 kHz AC signal superimposed on a DC voltage. For breakdown measurements, ohmic contacts to the β -Ga₂O₃ top surface were formed by aluminum wire bonding with indium contacts.⁹

Figures 1(b) and 1(c) show x-ray diffraction (XRD) data for a PdCoO₂/ β -Ga₂O₃ (001) heterostructure. XRD ϕ - χ scans of the PdCoO₂ (006) reflection, shown in Fig. 1(b), reveal that the PdCoO₂ (003L) planes are tilted with respect to the β -Ga₂O₃ (001) planes. Here, $\phi = \chi = 0^\circ$ corresponds to the alignment where the a -axis of the β -Ga₂O₃ (001) substrate is parallel to the projection of the x-ray detector arm on the substrate surface. The PdCoO₂ (006) reflection is observed at $\phi \approx 90^\circ$ and $\chi \approx 24^\circ$, indicating a 24° tilt of the PdCoO₂ (006) plane from the β -Ga₂O₃ (001) plane. These angles correspond to the dominant macroscopic epitaxial relationship of PdCoO₂ (006) // β -Ga₂O₃ (202). Consistently, the 2θ - ω scan along the PdCoO₂ (006) reflection in Fig. 1(c) shows both the PdCoO₂ (003L) and β -Ga₂O₃ (202) reflections. The tilted c -axis of the PdCoO₂ thin film results in a faceted surface morphology composed of PdCoO₂ c -plane facets, as confirmed by atomic force microscope (AFM) (Fig. S5). This epitaxial relationship can be understood based on the similar triangular arrangement of oxygen atoms on the PdCoO₂ (006) and β -Ga₂O₃ (202) surfaces (Fig. S3), which provides a structural basis for the observed alignment.

To examine the microscopic interfacial structure, high-angle annular dark field scanning transmission electron microscope (HAADF-STEM) image was captured around the PdCoO₂/ β -Ga₂O₃ interface, which is shown in Fig. 2. Due to Z -contrast, atomic columns with higher atomic numbers appear brighter in Fig. 2. Overall, a highly oriented crystalline interface was observed, showing chemical affinity between PdCoO₂ and β -Ga₂O₃. Alternating bright Pd and dark Co layers were clearly resolved, consistent with the crystal structure of PdCoO₂ shown in Fig. 1(a). This layered structure extended continuously near to the interface with β -Ga₂O₃ and also near

101 to the surface (Fig. S6). Some regions near the interface showed weak contrast, likely due to local
102 lattice tilting, interface roughness, and/or structural reconstruction. The presence of disorder near
103 the interface may locally alter the interfacial structure from the macroscopic epitaxial relationship
104 between PdCoO₂ (006) and β -Ga₂O₃ (202), which could lead to spatial variation in the Schottky
105 barrier height.

106 Closer inspection revealed stacking faults in the PdCoO₂ lattice, where twin boundaries (TBs)
107 are shown by green lines in Fig. 2. PdCoO₂ belongs to the rhombohedral $R\bar{3}m$ structure (3R
108 polytype), but local 2H polytype regions were occasionally observed at stacking faults,⁷ resulting
109 in 180° rotated domains around the c-axis of PdCoO₂. Although the impact of these stacking faults
110 on Schottky performance remains unclear, the Pd⁺/[CoO₂]⁻ stacking order was preserved,
111 suggesting minimal influence on the interface dipole.

112 The current density–voltage (J – V) characteristics of a circular PdCoO₂/ β -Ga₂O₃ junction (D
113 = 100 μ m) measured at varied temperature between $T = 298$ K and 573 K are shown in Fig. 3(a).
114 The PdCoO₂/ β -Ga₂O₃ junction showed rectifying J – V characteristics with reverse current density
115 as low as the noise level even at $T = 573$ K. The large on-off ratio $\sim 10^8$ at $T = 573$ K demonstrates
116 suitability of the PdCoO₂/ β -Ga₂O₃ (001) junction for diodes for high-temperature operation. The
117 forward J – V characteristics are shown in Fig. 3(b). We compare the forward J – V characteristics
118 with the thermionic emission model:

$$119 \quad J = A^{**}T^2 e^{-(\phi_b^{IV}/kT)} [e^{(qV/nkT)} - 1] \quad (\text{eq. 1})$$

120 where A^{**} is the effective Richardson constant, T is the temperature, q is the elementary charge,
121 and k is the Boltzmann constant. Here, $A^{**} \approx 41.1 \text{ A cm}^{-2} \text{ K}^{-2}$ for the theoretical effective mass $m^*/$
122 $m_0 = 0.342$ of β -Ga₂O₃.²³ Linear fitting of the forward J – V slope in the low J region (black lines
123 in Fig. 3(b)) and comparison with the eq. 1 yielded $\phi_b^{IV} = 1.74$ eV and an ideality factor $n = 1.06$
124 at $T = 298$ K, indicating that the electrical transport is well described by thermionic emission.

125 Similar behaviors are consistently observed in other $\text{PdCoO}_2/\beta\text{-Ga}_2\text{O}_3$ (001) junctions fabricated
126 on the same chip (Fig. S4).

127 Reported ϕ_b^{JV} values for Schottky junctions on $\beta\text{-Ga}_2\text{O}_3$ (001) are 1.09–1.46 eV for Pt
128 contacts,^{24,25} 0.99–1.22 eV for Ni contacts,²⁶ and 1.85 eV for PtO_x contacts.²⁷ The present PdCoO_2
129 electrode thus exhibits one of the highest SBHs among reported $\beta\text{-Ga}_2\text{O}_3$ (001) Schottky junctions,
130 likely consistent with the large work function on CoO_2 -terminated surface.¹³ The breakdown
131 voltage reached approximately $V_{\text{br}} = -530$ V as shown in Fig. S1 without edge termination or
132 trench isolation, showing the potential of $\text{PdCoO}_2/\beta\text{-Ga}_2\text{O}_3$ (001) interface for high-voltage
133 application. Further device engineering to relieve the electric field crowding may further improve
134 the breakdown voltages.^{25,28} The Schottky barrier height measured by C - V characteristics is ϕ_b^{CV}
135 = 2.10 eV at $T = 298$ K (Fig. S2). As typically observed, $\phi_b^{\text{CV}} > \phi_b^{\text{JV}}$, reflecting that C - V
136 measurements probe the spatial average of the barrier height, while J - V characteristics are
137 dominated by the lowest-barrier regions at the interface.²⁹ Consistently, the increase of ϕ_b^{JV} and
138 the decrease of n at higher temperature indicate the inhomogeneity of the SBH at the interface.
139 Assuming a simple Gaussian model and following the discussion by Werner and Güttler,³⁰ the
140 standard deviation σ_s of the Schottky barrier height can be estimated as,
141 $\sigma_s \approx \{2k_{\text{B}}T(\phi_b^{\text{CV}} - \phi_b^{\text{JV}})\}^{1/2}$. Using this formula, $\sigma_s = 143$ meV for the present $\text{PdCoO}_2/\beta\text{-Ga}_2\text{O}_3$
142 (001), which is comparable to the typical Schottky junctions on $\beta\text{-Ga}_2\text{O}_3$.³¹ It should be noted that
143 the structural complexity of the interface, as seen in the HAADF-STEM image, limits the
144 discussion based on the simple Gaussian distribution.

145 In the J - V characteristics in Fig. 3(b), the current density saturates at higher forward biases,
146 resulting in a large on-state resistance (R_{on}). This behavior is likely caused by limited current
147 spreading in the PdCoO_2 electrode. PdCoO_2 is known to exhibit strong anisotropy in resistivity:
148 $\rho_c = 1.07$ m Ω cm and $\rho_{\text{ab}} = 2.6$ $\mu\Omega$ cm for the c -axis direction and the ab -plane direction at $T =$

149 300 K.⁶ This gives the resistivity ratio as high as $\rho_c/\rho_{ab} \sim 400$. We patterned the PdCoO₂ thin film
 150 on β -Ga₂O₃ (001) into Hall-bar geometry and measured the resistivity along different directions.
 151 As shown in Fig. S7, the resistivity along the direction intersecting the PdCoO₂ (006) facets is
 152 consistently higher than that along the facet surfaces. Thus, the high resistivity along the *c*-axis
 153 can hinder efficient lateral current spreading across the contact area. To examine this effect, we
 154 deposited an Au (150 nm)/Ni (30 nm) current-spreading electrode on PdCoO₂ and measured the
 155 *J-V* characteristics as shown in Fig. 4(a). Without the Au/Ni layer, R_{on} increases with increasing
 156 diode diameter *D*, reflecting the longer spreading distance from the needle probe contact point
 157 (gray plot in Fig. 4(b)). In contrast, the Au/Ni current-spreading electrode significantly reduces
 158 R_{on} (green plot in Fig. 4(b)), although Au/Ni thermal stability is insufficient for high-temperature
 159 operation. Developing thermally stable current-spreading electrodes will therefore be important
 160 to achieve both high-temperature operation and low R_{on} . Figure 4(c) summarizes the device-to-
 161 device distribution of the Schottky barrier height ϕ_b^{JV} extracted from *J-V* characteristics and the
 162 ideality factor *n*, demonstrating good reproducibility of $\phi_b^{JV} > 1.7$ eV and *n* close to unity. The
 163 observed spread in ϕ_b^{JV} and *n* could reflect local variations in the interface structure, defect density,
 164 and quality of PdCoO₂.

165 As a possible mechanism of high Schottky barrier formation, interface dipole effects proposed
 166 in PdCoO₂/ β -Ga₂O₃ ($\bar{2}01$) may also be relevant.⁴ For β -Ga₂O₃ ($\bar{2}01$), the interface dipole of
 167 PdCoO₂ was oriented normal to the interface,⁴ whereas in the present (001) system, the dipole is
 168 tilted by $\chi = 24^\circ$. The perpendicular component ($\cos\chi = 0.91$) is nearly equivalent to the vertical
 169 case, suggesting that the dipole effect remains non-negligible. However, if both Pd and CoO₂
 170 layers extend to the interface, periodic stripe-like potential modulation may arise. Although the
 171 temperature dependence of ϕ_b^{JV} and *n* indicate barrier inhomogeneity, such behavior is commonly
 172 observed in various Schottky junctions and cannot be the direct evidence for the periodic potential
 173 modulation. In fact, the periodicity of this stripe is estimated to be $c/3 \times 1/\cos\chi = 0.65$ nm—much

This is the author's peer reviewed, accepted manuscript. However, the online version of record will be different from this version once it has been copyedited and typeset.

PLEASE CITE THIS ARTICLE AS DOI: 10.1063/5.0332733

174 smaller than the depletion width $W \approx 520$ nm corresponding to $\phi_b^{\text{CV}} = 2.10$ eV and $N_D = 7.8 \times 10^{15}$
175 cm^{-3} . The large depletion width W suppresses the short-range modulation of the band bending in
176 $\beta\text{-Ga}_2\text{O}_3$. Thus, the interface likely behaves effectively as a spatially averaged Schottky barrier
177 rather than a collection of local high barriers and leaky low barriers even if stripe-like potential
178 modulation existed. Such averaging effect of nanoscale potential distribution has been discussed
179 in $\text{SrRuO}_3/\text{Nb:SrTiO}_3$ Schottky junctions with a fractionally inserted $(\text{AlO}_2)^-(\text{LaO})^+$ dipole
180 layer.³² The observed $\phi_b^{\text{CV}} = 2.10$ eV exceeds the value predicted from the experimentally
181 observed work function dependence of ϕ_b and the average work function $\phi_m^{\text{average}} = (\phi_m^{\text{Pd}} +$
182 $\phi_m^{\text{CoO}_2})/2 = 6.25$ eV, expected from the work functions for Pd- ($\phi_m^{\text{Pd}} = 4.7$ eV)^{4,13} and CoO_2 -
183 terminated surfaces ($\phi_m^{\text{CoO}_2} = 7.8$ eV).¹³ The observed ϕ_b^{CV} and qV_{bi} rather closely match that of
184 CoO_2 termination on $(\bar{2}01)$ ($qV_{\text{bi}} = 2.0$ eV).⁴ This suggests that the simple averaging model is
185 insufficient to explain the observed barrier height, and the microscopic interfacial structure likely
186 plays a crucial role. The HAADF-STEM image shows reduced Pd-layer contrast near the interface,
187 implying a locally modified layered structure distinct from bulk PdCoO_2 . As reported for $\text{PtO}_x/\beta\text{-}$
188 Ga_2O_3 interfaces, oxygen-mediated bonding may be important at the interface.²⁷

189 In addition, the electronic states of PdCoO_2 are strongly layer-dependent. Previous studies
190 have shown that the Pd-derived states near the Fermi level are primarily associated with in-plane
191 Pd-Pd metallic bonding.³³ The CoO_2 layers, on the other hand, are associated with more correlated
192 electronic states involving Co 3d-O 2p hybridized states.³³ Such differences could result in
193 distinct contributions of Pd- and CoO_2 -derived states to electronic transport across $\text{PdCoO}_2/\beta\text{-}$
194 Ga_2O_3 interface. In particular, at an oxide interface where bonding is mediated by oxygen, CoO_2 -
195 like configurations could couple more effectively to $\beta\text{-Ga}_2\text{O}_3$ through oxygen-mediated
196 interactions. This may result in an effective barrier height that deviates from a simple spatial
197 averaging of Pd- and CoO_2 -terminated regions. Further theoretical and experimental studies are
198 needed to elucidate the atomic-scale interface and the potential distribution when a layered oxide

199 with surface dipoles contacts an oxide semiconductor at an oblique angle.

200 In summary, we fabricated heterostructures of conductive layered oxide PdCoO₂ and β -Ga₂O₃
 201 (001). The PdCoO₂ thin film was found to grow dominantly with the epitaxial relationship
 202 PdCoO₂ (006) // β -Ga₂O₃ (202), with the PdCoO₂ surface polarization direction tilted by $\sim 24^\circ$
 203 from the β -Ga₂O₃ (001) surface normal. Nevertheless, a large Schottky barrier height exceeding
 204 1.7 eV was obtained at the PdCoO₂/ β -Ga₂O₃ (001) interface, enabling current rectification at
 205 elevated temperatures. This demonstrates that the advantage of PdCoO₂ electrodes—such as its
 206 strong dipole-induced high work function and high-quality oxide–oxide interface—can be usable
 207 on β -Ga₂O₃ (001)-based heterostructures. Further optimization of device design, such as edge
 208 termination²⁵ and/or trench structures²⁸ is needed to enable high-voltage and high-temperature
 209 operation utilizing PdCoO₂/ β -Ga₂O₃ crystalline heterostructures.

210

211 SUPPLEMENTARY MATERIAL

212 Figures S1-S7 are available in the supplementary material.

213

214 **ACKNOWLEDGEMENTS:** A part of this work was supported by ARIM of MEXT
 215 (JPMXP1223NM5155), MEXT Leading Initiative for Excellent Young Researchers
 216 (JPMXS0320200047), JST PRESTO (JPMJPR20AD), and Grant-in-Aid for Scientific Research
 217 (B) from JSPS (24K01353).

218

219 REFERENCE

- 220 ¹ M. Higashiwaki, K. Sasaki, H. Murakami, Y. Kumagai, A. Koukitu, A. Kuramata, T.
 221 Masui, and S. Yamakoshi, *Semicond. Sci. Technol.* **31**, 034001 (2016); S. J.
 222 Pearton, J. Yang, P. H. Cary IV, F. Ren, J. Kim, M. J. Tadjer, and M. A. Mastro, *Applied*
 223 *Physics Reviews* **5**, 011301 (2018); S. J. Pearton, F. Ren, M. Tadjer, and J. Kim, *J.*
 224 *Appl. Phys.* **124**, 220901 (2018).

This is the author's peer reviewed, accepted manuscript. However, the online version of record will be different from this version once it has been copyedited and typeset.

PLEASE CITE THIS ARTICLE AS DOI: 10.1063/5.0332733

- 225 ² S. Oh, G. Yang, and J. Kim, *ECS Journal of Solid State Science and Technology* **6** (2),
226 Q3022 (2017).
- 227 ³ C. Hou, R. A. Makin, K. R. York, S. M. Durbin, J. I. Scott, R. M. Gazoni, R. J. Reeves,
228 and M. W. Allen, *Appl. Phys. Lett.* **114** (23) (2019); C. Hou, R. M. Gazoni, R. J.
229 Reeves, and M. W. Allen, *Appl. Phys. Lett.* **114**, 033502 (2019); E. Farzana, S. Roy,
230 N. S. Hendricks, S. Krishnamoorthy, and J. S. Speck, *Appl. Phys. Lett.* **123** (19) (2023).
- 231 ⁴ T. Harada, S. Ito, and A. Tsukazaki, *Sci. Adv.* **5**, eaax5733 (2019).
- 232 ⁵ R. D. Shannon, D. B. Rogers, and C. T. Prewitt, *Inorg. Chem.* **10**, 713 (1971);
233 R. Daou, R. Frésard, V. Eyert, S. Hébert, and A. Maignan, *Sci. Technol. Adv. Mater.*
234 **18**, 919 (2017).
- 235 ⁶ A. P. Mackenzie, *Rep. Prog. Phys.* **80**, 032501 (2017).
- 236 ⁷ T. Harada, *Mater. Today Adv.* **11**, 100146 (2021).
- 237 ⁸ V. Sunko, H. Rosner, P. Kushwaha, S. Khim, F. Mazzola, L. Bawden, O. J. Clark, J. M.
238 Riley, D. Kasinathan, M. W. Haverkort, T. K. Kim, M. Hoesch, J. Fujii, I. Vobornik, A. P.
239 Mackenzie, and P. D. C. King, *Nature* **549**, 492 (2017); F. Mazzola, V. Sunko, S.
240 Khim, H. Rosner, P. Kushwaha, O. J. Clark, L. Bawden, I. Marković, T. K. Kim, M.
241 Hoesch, A. P. Mackenzie, and P. D. C. King, *Proc. Natl. Acad. Sci. U.S.A.* **115**, 12956
242 (2018); T. Harada, K. Sugawara, K. Fujiwara, M. Kitamura, S. Ito, T. Nojima, K.
243 Horiba, H. Kumigashira, T. Takahashi, T. Sato, and A. Tsukazaki, *Phys. Rev. Res.* **2**,
244 013282 (2020); Q. Song, J. Sun, C. T. Parzyck, L. Miao, Q. Xu, F. V. E. Hensling, M.
245 R. Barone, C. Hu, J. Kim, B. D. Faeth, H. Paik, P. D. C. King, K. M. Shen, and D. G.
246 Schlom, *APL Mater.* **10**, 091113 (2022).
- 247 ⁹ T. Harada and A. Tsukazaki, *APL Mater.* **8**, 041109 (2020).
- 248 ¹⁰ T. Harada and A. Tsukazaki, *Appl. Phys. Lett.* **116**, 232104 (2020).
- 249 ¹¹ T. Miyakawa, T. Harada, S. Ito, and A. Tsukazaki, *J. Appl. Phys.* **128**, 025302 (2020);
250 R. Wei, C. Gao, Y. Meng, L. Zhu, J. Zhang, L. Hu, L. Li, X. Zhu, X. Zhu, and Y. Sun,
251 *Appl. Phys. Lett.* **128** (2) (2026).
- 252 ¹² P. W. Tasker, *J. Phys. C: Solid State Phys.* **12**, 4977 (1979).
- 253 ¹³ C. M. Yim, D. Chakraborti, L. C. Rhodes, S. Khim, A. P. Mackenzie, and P. Wahl, *Sci.*
254 *Adv.* **7**, eabd7361 (2021).
- 255 ¹⁴ T. Harada and Y. Okada, *APL Mater.* **10**, 070902 (2022).
- 256 ¹⁵ T. Harada, K. Fujiwara, and A. Tsukazaki, *APL Mater.* **6**, 046107 (2018).
- 257 ¹⁶ P. Yordanov, W. Sigle, P. Kaya, M. E. Gruner, R. Pentcheva, B. Keimer, and H.-U.
258 Habermeier, *Phys. Rev. Mater.* **3**, 085403 (2019).
- 259 ¹⁷ M. Brahlek, G. Rimal, J. M. Ok, D. Mukherjee, A. R. Mazza, Q. Lu, H. N. Lee, T. Z.

This is the author's peer reviewed, accepted manuscript. However, the online version of record will be different from this version once it has been copyedited and typeset.

PLEASE CITE THIS ARTICLE AS DOI: 10.1063/5.0332733

- 260 Ward, R. R. Unocic, G. Eres, and S. Oh, *Phys. Rev. Mater.* **3**, 093401 (2019); J.
- 261 Sun, M. R. Barone, C. S. Chang, M. E. Holtz, H. Paik, J. Schubert, D. A. Muller, and D.
- 262 G. Schlom, *APL Mater.* **7**, 121112 (2019).
- 263 ¹⁸ R. Wei, P. Gong, M. Zhao, H. Tong, X. Tang, L. Hu, J. Yang, W. Song, X. Zhu, and Y.
- 264 Sun, *Adv. Funct. Mater.* **30**, 2002375 (2020).
- 265 ¹⁹ P. F. Carcia, R. D. Shannon, P. E. Bierstedt, and R. B. Flippen, *J. Electrochem. Soc.* **127**,
- 266 1974 (1980); T. Harada, T. Nagai, M. Oishi, and Y. Masahiro, *J. Appl. Phys.* **133**,
- 267 085302 (2023); T. Harada, Z. P. L. Ang, Y. Sakakibara, T. Nagai, and Y. Masahiro,
- 268 *Appl. Phys. Lett.* **126** (22), 221902 (2025); T. Harada, Y. Iwai, M. Abe, T. Nagai, Y.
- 269 Masahiro, and Y. Kama, presented at the 2025 IEEE International Interconnect
- 270 Technology Conference (IITC), 2025.
- 271 ²⁰ P. Mazzolini, A. Falkenstein, C. Wouters, R. Schewski, T. Markurt, Z. Galazka, M. Martin,
- 272 M. Albrecht, and O. Bierwagen, *APL Mater.* **8** (1) (2020).
- 273 ²¹ H. Murakami, K. Nomura, K. Goto, K. Sasaki, K. Kawara, Q. T. Thieu, R. Togashi, Y.
- 274 Kumagai, M. Higashiwaki, A. Kuramata, S. Yamakoshi, B. Monemar, and A. Koukitu,
- 275 *Applied Physics Express* **8** (1), 015503 (2015).
- 276 ²² C.-C. Chiang, X. Xia, J.-S. Li, F. Ren, and S. J. Pearton, *ECS Journal of Solid State*
- 277 *Science and Technology* **11** (11), 115005 (2022).
- 278 ²³ H. He, R. Orlando, M. A. Blanco, R. Pandey, E. Amzallag, I. Baraille, and M. Rérat,
- 279 *Phys. Rev. B* **74**, 195123 (2006).
- 280 ²⁴ M. Higashiwaki, K. Konishi, K. Sasaki, K. Goto, K. Nomura, Q. T. Thieu, R. Togashi, H.
- 281 Murakami, Y. Kumagai, B. Monemar, A. Koukitu, A. Kuramata, and S. Yamakoshi,
- 282 *Appl. Phys. Lett.* **108**, 133503 (2016).
- 283 ²⁵ K. Konishi, K. Goto, H. Murakami, Y. Kumagai, A. Kuramata, S. Yamakoshi, and M.
- 284 Higashiwaki, *Appl. Phys. Lett.* **110**, 103506 (2017).
- 285 ²⁶ T. Oshima, A. Hashiguchi, T. Moribayashi, K. Koshi, K. Sasaki, A. Kuramata, O. Ueda,
- 286 T. Oishi, and M. Kasu, *Jpn. J. Appl. Phys.* **56** (8), 086501 (2017); J. Yang, C.
- 287 Fares, F. Ren, R. Sharma, E. Patrick, M. E. Law, S. J. Pearton, and A. Kuramata, *J. Appl.*
- 288 *Phys.* **123** (16) (2018).
- 289 ²⁷ G. Jian, W. Hao, Z. Shi, Z. Han, K. Zhou, Q. Liu, Q. He, X. Zhou, C. Chen, Y. Zhou, X.
- 290 Zhao, G. Xu, and S. Long, *J. Phys. D: Appl. Phys.* **55** (30), 304003 (2022).
- 291 ²⁸ W. Li, Z. Hu, K. Nomoto, Z. Zhang, J.-Y. Hsu, Q. T. Thieu, K. Sasaki, A. Kuramata, D.
- 292 Jena, and H. G. Xing, *Appl. Phys. Lett.* **113** (20) (2018).
- 293 ²⁹ R. T. Tung, *Applied Physics Reviews* **1**, 011304 (2014).
- 294 ³⁰ J. H. Werner and H. H. Güttler, *J. Appl. Phys.* **69**, 1522 (1991).

This is the author's peer reviewed, accepted manuscript. However, the online version of record will be different from this version once it has been copyedited and typeset.

PLEASE CITE THIS ARTICLE AS DOI: 10.1063/5.0332733

295 ³¹ G. Jian, Q. He, W. Mu, B. Fu, H. Dong, Y. Qin, Y. Zhang, H. Xue, S. Long, Z. Jia, H. Lv,
296 Q. Liu, X. Tao, and M. Liu, *AIP Advances* **8**, 015316 (2018).
297 ³² T. Yajima, M. Minohara, C. Bell, H. Y. Hwang, and Y. Hikita, *Appl. Phys. Lett.* **113**,
298 221603 (2018).
299 ³³ Q. Lu, H. Martins, J. M. Kahk, G. Rimal, S. Oh, I. Vishik, M. Brahlek, W. C. Chueh, J.
300 Lischner, and S. Nemsak, *Communications Physics* **4** (1), 143 (2021).
301

This is the author's peer reviewed, accepted manuscript. However, the online version of record will be different from this version once it has been copyedited and typeset.

PLEASE CITE THIS ARTICLE AS DOI: 10.1063/5.0332733

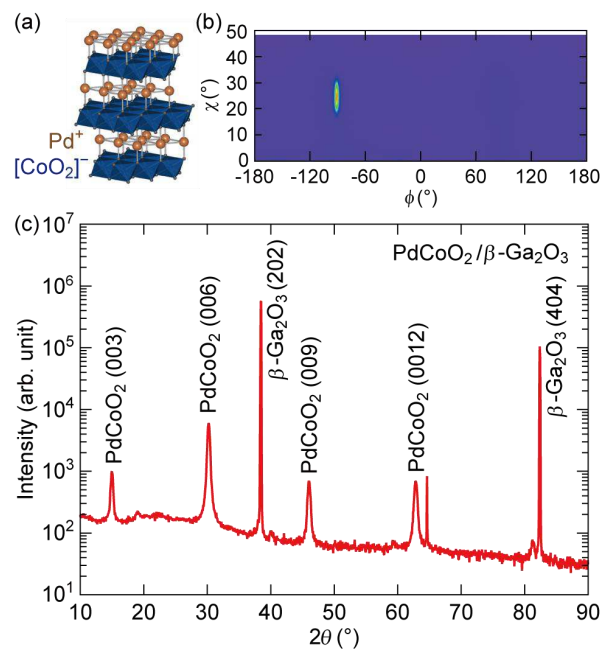
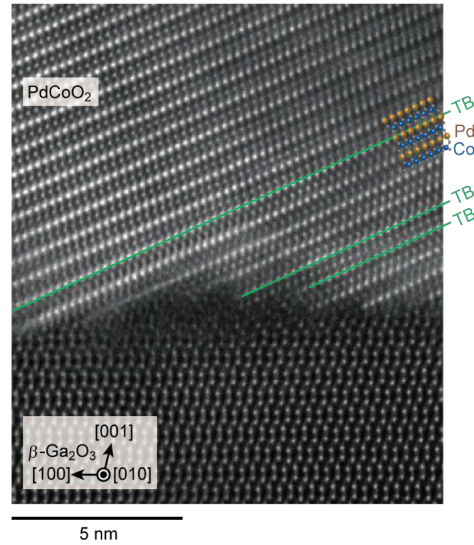


FIG. 1. (a) Crystal structure of PdCoO₂ highlighting the alternating ionic layers of Pd⁺ and [CoO₂]⁻. (b) XRD ϕ - χ mapping of PdCoO₂/β-Ga₂O₃ (001). (c) XRD 2 θ - ω scan of PdCoO₂/β-Ga₂O₃ (001) along the reciprocal vector \mathbf{G}_{003n} of PdCoO₂, measured in asymmetric geometry.

This is the author's peer reviewed, accepted manuscript. However, the online version of record will be different from this version once it has been copyedited and typeset.

PLEASE CITE THIS ARTICLE AS DOI: 10.1063/5.0332733

308
309



310

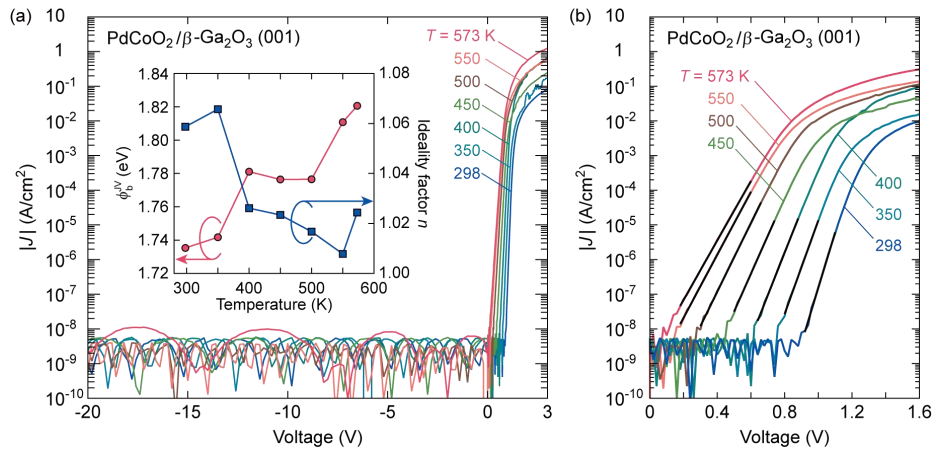
311 **FIG. 2.** HAADF-STEM image of a PdCoO₂/β-Ga₂O₃ (001) interface. The crystal model of
312 PdCoO₂ is overlapped in the HAADF-STEM image. Twin boundaries (TBs) in the stacking faults
313 are indicated by green lines.

This is the author's peer reviewed, accepted manuscript. However, the online version of record will be different from this version once it has been copyedited and typeset.

PLEASE CITE THIS ARTICLE AS DOI: 10.1063/5.0332733

314

315



316

317 **FIG. 3.** (a) Temperature-dependent current density-voltage characteristics of a PdCoO₂/β-Ga₂O₃
318 (001) heterostructure. The noted numbers are the stage temperature (T) during the J - V
319 measurement. Inset: Schottky barrier height determined by the J - V characteristics (ϕ_b^{JV} , red
320 circles) and the ideality factor (n , blue squares) at varied temperature. (b) Forward J - V
321 characteristics of a PdCoO₂/β-Ga₂O₃ (001) heterostructure with the fitting lines at the linear region
322 (black lines). The ϕ_b^{JV} and n are determined from the fitting lines by thermionic emission model
323 (eq. 1).

This is the author's peer reviewed, accepted manuscript. However, the online version of record will be different from this version once it has been copyedited and typeset.

PLEASE CITE THIS ARTICLE AS DOI: 10.1063/5.0332733

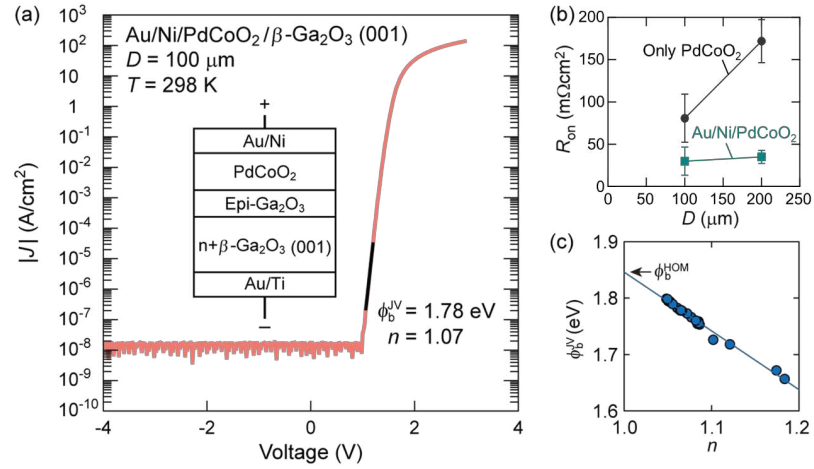


FIG. 4. (a) J - V characteristics of Au/Ni/PdCoO₂/β-Ga₂O₃ (001) Schottky junction at $T = 298$ K. The inset is the schematics of the device structure. (b) Dependence of on-state resistance (R_{on}) on diode diameter (D) for PdCoO₂-only and Au/Ni/PdCoO₂ contacts. Each data point represents the average of multiple devices ($N \geq 5$ for PdCoO₂-only and $N \geq 10$ for Au/Ni/PdCoO₂ contacts), and the error bars indicate the standard deviation. (c) The ϕ_b^{JV} versus n plot for Au/Ni/PdCoO₂/β-Ga₂O₃ (001) Schottky junctions with $D = 100$ μm at $T = 298$ K for the number of the devices $N = 25$, fabricated on the same wafer in a single process flow. The blue line is the linear fitting to the ϕ_b^{JV} versus n plot, which intersects the $n = 1.0$ line at $\phi_b^{HOM} \simeq 1.85$ eV.